Theoretical Study of Ammonolysis of Monobactams: Kinetic Role of the *N*-Sulfonate Group

Natalia Díaz, **Dimas Suárez** and **Tomás L. Sordo***

Departamento de Química Física y Analítica. Universidad de Oviedo, Julián Clavería 8, E-33006 Oviedo, Asturias (Phone: +34-985103475; fax: +34-985103125; e-mail: tsordo@correo.uniovi.es)

The ammonolysis reaction of 3-(formylamino)-4-methyl-2-oxoazetidine-1-sulfonate is investigated by quantum-chemical methods (B3LYP/6-31 + G*) as a model system of the aminolysis reaction of monobactam antibiotics involved in the allergic reaction to these drugs. The influence of the *N*-sulfonate group on the β-lactam ring, reaction intermediates, and transition states is characterized in terms of the geometries and relative energies of the corresponding critical structures located on the B3LYP/6-31 + G* potential-energy surface. It is shown that the *N*-sulfonate group, which has only a moderate impact on the structure and charge distribution of the β-lactam ring, reduces the rate-determining ΔG barrier by *ca.* 20 kcal/mol with respect to a purely uncatalyzed ammonolysis of the unsubstituted system, azetidin-2-one. This intramolecular catalytic effect occurs through a $-NH-SO_3^- \leftrightarrow [-N-SO_3H]^-$ isomerization process, which is involved in the proton relay from the attacking ammonia molecule to the β-lactam N-atom. Our theoretical results predict that, in aqueous solution, monobactams will show an intrinsic reactivity against amine nucleophiles more important than that of penicillins.

1. Introduction. – The aminolysis of β-lactam antibiotics is a substitution reaction at the carbonyl group of the β-lactam ring involved in the biochemical activity of these substances [1]. The problem of allergy to β-lactam drugs, which is the main factor limiting their use, is determined by the formation of covalent amide bonds between β-lactams and plasmid proteins like human serum albumin (HSA) [2]. The aminolysis of penicillins by ε-amino groups of reactive lysine residues in HSA yields the penicilloyl group which is considered as the major antigenic determinant of penicillin allergy [2] detected by the immune system. Therefore, one of the reagents included in allergy skin tests for the determination of antibodies to β-lactam antibiotics is the penicilloyl group resulting from the aminolysis of β-lactams with polylysine or HSA carrier molecules [3]. To further understand this biochemical process, the aminolysis of β-lactam compounds has been studied both experimentally [4–8] and theoretically [9][10].

Monobactams [11] are monocyclic β-lactam antibiotics characterized by the presence of a strongly acidic sulfonate group at the N(1) position. Aztreonam (**1**) is the first monobactam of this modern class of antibiotics [12] to be marketed. Common interpretations are based on the assumption that the electron-withdrawing ability of the deprotonated *N*-sulfonate group activates the β-lactam ring as does geometric constraint in bicyclic β-lactams. Nevertheless, monobactams present particular characteristics in their mode of action and activity compared with that of bicyclic antibiotics. First, the antibacterial spectrum of monobactams is limited to aerobic *Gram*-negative bacilli, lacking thus affinity for the essential penicillin-binding proteins of *Gram*-positive bacteria and anaerobic organisms [12]. Monobactams show, in

general, a high degree of stability toward the hydrolytic action of β-lactamases, although some β-lactamases from *Klebsiella* and *Pseudomonas aureginosa* microorganisms have resulted in aztreonam resistance [12]. Most interestingly, metallo-β-lactamases, which have become a prominent class of enzymes hydrolyzing a broad spectrum of β-lactams [13], manifest a relatively low activity against these monocyclic antibiotics [14]. On the other hand, monobactams bridged across the C(3)–C(4) bond have been reported as potent mechanism-based inhibitors of class C β-lactamases [15]. Finally, although aztreonam also forms amide linkages to HSA under physiological conditions [16], monobactam drugs are weakly immunogenic and display very low immunological cross-reactivity reactions with other β-lactams like penicillins or cephalosporins [12][17][18].

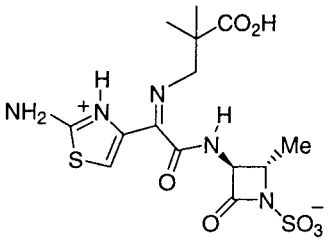

1

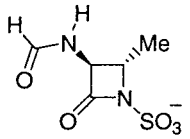

2

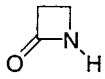

3

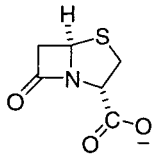

4

For further investigation of the substituent effects of β-lactams, monobactams are very interesting candidate systems to be studied theoretically. In this work, we report a quantum-chemical investigation of the ammonolysis reaction of the monobactam model compound **2**. The study of this particular model reaction will provide structural and energetic data most suitable for comparison with those obtained in previous theoretical work on the aminolysis/ammonolysis of azetidin-2-one (**3**) and penicillin models like 3α-carboxypenam (**4**) [9][10]. This comparison will allow us to display the intrinsic effects produced by the *N*-sulfonate group on these processes and to gain some insight into the differences in structure and function between the monocyclic and bicylic β-lactam antibiotics. Particularly, the implications of the results for understanding the immunochemistry of monobactams will be discussed.

2. Methods. – Molecular-geometry optimizations, followed by analytical frequency calculations, were performed at the HF/3-21G* and B3LYP/6-31 + G* levels of theory [19][20] with the GAUSSIAN98 suite of programs [21]. Although the preliminary HF/3-21G* results are not presented in this work, intrinsic reaction coordinate (IRC) calculations [22] at the HF/3-21G* level were carried out to confirm the reaction paths on the potential-energy surface (PES) connecting the different transition structures (TS), intermediates, and products. The geometry of the reactive bonds (*e.g.*, the forming/breaking C–N bonds) in the different TSs were quite similar ($\pm$0.05 Å) at the HF/3-21G* and B3LYP/6-31 + G* levels, while H-bond contacts were *ca.* 0.2 Å shorter at HF/3-21G*. $\Delta G_{\text{gas-phase}}$ Values were obtained by combining the B3LYP/6-31 + G* electronic energies and thermal corrections [23] at the same level of theory.

To calibrate the B3LYP/6-31 + G* level of theory used in this work, we also studied the gas-phase protonation of methanesulfonate and the conversion of the $NH_2-SO_3^-$ species to the $[NH-SO_3H]^-$ isomer at the MP2/6-31 + G* and B3LYP/6-31 + G* levels. Electronic energies for the MP2/6-31 + G*-optimized structures were recomputed with the G2(MP2,SVP) scheme [24], while ZPVE and thermal corrections are taken from B3LYP/6-31 + G* frequencies. The G2(MP2,SVP) scheme, which reproduces the thermochemical data of the G2 test set with an average absolute deviation of 1.63 kcal/mol, approximates the sophisticated QCISD(T)/6-311 + G(3df,2p) level of theory in an additive fashion as follows:

$$E[\text{QCISD(T)/6-311+G(3df,2p)}] \approx E[\text{G2(MP2,SVP)}] = E[\text{QCISD(T)/6-31G*}] + E[\text{MP2/6-311+G(3d f,2p)}] - E[\text{MP2/6-31G*}]$$

To take into account condensed-phase effects on the kinetics and thermodynamics of the reaction, we used the UAHF (united-atom *Hartree-Fock*) parameterization [25] of the polarizable continuum model [26] (PCM), including both electrostatic and non-electrostatic solute-solvent interactions and simulating H_2O as solvent. The solvation *Gibbs* energies $\Delta G_{\text{solvation}}$ of all the critical structures were then computed from single-point B3LYP/6-31 + G* PCM-UAHF calculations on the B3LYP/6-31 + G* gas-phase geometries. Addition of the relative solvation *Gibbs* energies to the $\Delta G_{\text{gas-phase}}$ values gives the $\Delta G_{\text{solution}}$ values in the *Table*.

Table. *Relative Energies [kcal/mol] for the Ammonolysis Reaction of 3-(Formylamino)-4-methyl-2-oxoazetidine-1-sulfonate.* Values in parentheses correspond to the ammonolysis reaction of azetidin-2-one (see also [9]).

	B3LYP/6-31 + G* [a])	$\Delta G_{\text{gas-phase}}$ [b])	$\Delta\Delta G_{\text{solvation}}$ [c])	$\Delta G_{\text{solution}}$ [d])
Reactants	0.0	0.0	0.0	0.0
C	−4.4 (−2.6)	4.8 (4.0)	6.5 (5.4)	11.3 (9.4)
TS_c	43.1 (46.6)	54.2 (56.5)	−4.2 (1.8)	50.0 (58.3)
P_c	−20.9 (−19.2)	−10.0 (−9.8)	2.7 (2.6)	−7.3 (−7.1)
TS_1	41.7 (47.8)	53.7 (58.1)	0.1 (0.2)	53.8 (58.3)
I_1	3.5 (14.9)	15.3 (25.4)	6.2 (3.7)	21.5 (29.1)
TS_2	33.5 (43.3)	45.3 (53.2)	6.2 (4.0)	51.5 (57.3)
P_2	−19.9 (−17.1)	−8.4 (−8.4)	3.8 (1.4)	−4.6 (−7.0)
TS_3	12.8	24.9	6.0	30.9
I_2	0.2	10.7	4.5	15.2
TS_i	4.5	16.4	4.5	20.9
I_3	4.3	15.3	4.0	19.3
TS_4	18.7	30.1	10.1	40.2
TS_5	25.7	37.2	−1.4	35.8
I_4	25.6	37.0	−1.4	35.6
TS_6	25.6	37.6	−2.0	35.6
I_5	7.1	17.1	−3.6	13.5
I_6	5.2	16.6	−1.8	14.8
TS_7	20.6	31.9	7.8	39.7
P_3	−22.2	−10.4	5.9	−4.5

[a]) Including ZPVE correction from B3LYP/6-31 + G* frequencies. [b]) Based on B3LYP/6-31 + G* electronic energies and thermal corrections. [c]) Relative $\Delta G_{\text{solvation}}$ with respect to reactants from single-point B3LYP/6-31 + G* PCM-UAHF calculations. [d]) $\Delta G_{\text{solution}} = \Delta G_{\text{gas-phase}} + \Delta\Delta G_{\text{solvation}}$.

The SCRF calculations were carried out on the gas-phase geometries given that, in a previous work on the aminolysis reaction of azetidin-2-one [9], we found similar optimized geometries both in the gas phase and in solution. Furthermore, in the same work [9], the relative $\Delta G_{solvation}$ values for the structures along the reaction energy profile were practically identical regardless of the geometries used (*i.e.*, the gas-phase geometries or the solvated ones). We also note that the ability of the PCM method to study solute-solvent interactions in charged systems has been tested in the S_N2 model reaction $CH_3Cl + Cl^- \rightarrow Cl^- + CH_3Cl$, in which the PCM reaction energy profile and the barrier height compare satisfactorily with those obtained in molecular simulation studies [27].

Atomic charges were computed, carried out on a natural population analysis [28] (NPA) with the corresponding B3LYP/6-31 + G* density matrices.

For comparison purposes, the most important critical structures determined in our previous study on the ammonolysis of azetidin-2-one [9] were reoptimized at the B3LYP/6-31 + G* level, followed by the corresponding frequency calculations and single-point B3LYP/6-31 + G* PCM-UAHF calculations.

Results and Discussion. – 3.1. *Test Calculations.* The ability of the B3LYP method to study the aminolysis of the simplest β-lactam azetidin-2-one (**3**) has been tested extensively in [9][10] by comparing favorably the B3LYP results with those performed at higher levels of theory. However, to further calibrate the methodology to be used in the determination of the influence of the sulfonate group in the energetics of the ammonolysis of monobactams, the proton affinity (PA) of the methanesulfonate anion and the reaction profile for the $NH_2-SO_3^- \rightarrow [NH-SO_3H]^-$ isomerization were investigated at the MP2/6-31 + G* level and at B3LYP/6-31 + G*, the electronic energies being recomputed at the G2(MP2,SVP) level on the MP2/6-31 + G* geometries. The methanesulfonate compound has a PA of 316.1 kcal/mol at B3LYP/6-31 + G*, which is quite close to the high-level G2 value of 318.0 kcal/mol. The energetics of the $NH_2-SO_3^- \rightarrow [NH-SO_3H]^-$ process may constitute a more interesting reference. The calculated energy barrier for this 1,3 H-shift amounts to 39.6 and 40.4 kcal/mol at the B3LYP/6-31 + G* and the G2-like levels of theory, respectively. The corresponding reaction energies are also very similar, 21.5 kcal/mol (B3LYP/6-31 + G*) and 20.6 kcal/mol (G2), respectively, and predict unequivocally that the $[NH-SO_3H]^-$ isomer is much less stable than the $NH_2-SO_3^-$ form. We conclude that the application of the B3LYP/6-31 + G* level to study the title reaction represents a good compromise between accuracy and computational cost.

3.2. *Geometry and Charge Distribution of β-Lactam Models. Fig. 1* shows the B3LYP/6-31 + G* equilibrium geometry of various β-lactam models: 3-(formylamino)-4-methylazetidin-2-one, 3α-carboxypenam (a penicillin model), and 3-(formylamino)-4-methyl-2-oxoazetidine-1-sulfonate (a monobactam model).

At B3LYP/6-31 + G*, the geometry of the monobactam model presents an endocylic N-atom with low pyramidalization, the sum of the X–N–Y angles being 353 degrees (358 degrees in the crystal structure of aztreonam described in reference 29). We also note that the S–N (1.804 Å) and the S=O (*ca.* 1.48 A) bond lengths are quite dissimilar, reflecting clearly single- and double-bond character, respectively.

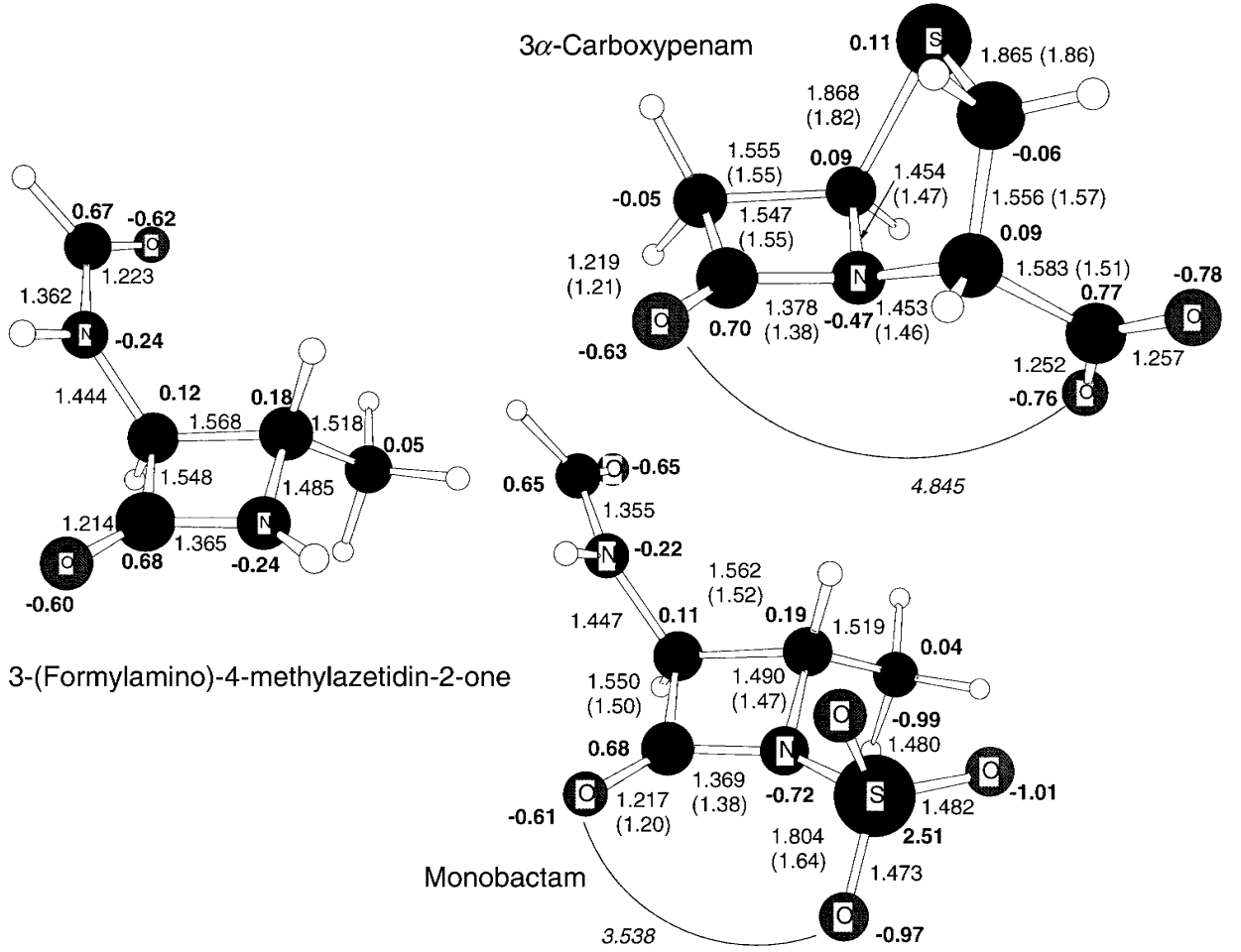

Fig. 1. *B3LYP/6-31 + G* Optimized structures for some β-lactam model compounds.* Distances in Å. B3LYP/6-31 + G* NPA Atomic charges in bold characters. Some X-ray bond distances are indicated in parentheses as reported for aztreonam[1]) and benzylpenicillin [30].

[1]) We note that the *N*-sulfonate group forms two salt-bridge contacts with neighboring aztreonam molecules in the crystal structure (see [29]).

The electron-withdrawing effect of the SO_3^- group is commonly thought to decrease the amide resonance. This hypothetical inductive effect is not so reflected in the C=O and C–N monobactam amide bond lengths, which are practically equal to those of 3-(formylamino)-4-methylazetidin-2-one. The NPA charge of the azetidin-2-one and the monobactam models, after subtracting the contribution of the N–H and N–SO_3 moieties, amounts to +0.24 e and +0.18 e, respectively. Thus, from the geometry and charge distribution of the monobactam model, it is clear that the SO_3^- group hardly has an electron-withdrawing effect, so that the amide resonance structures, $\mathbf{I_A}$ and $\mathbf{II_A}$ in *Scheme 1*, may account well for the electronic structure. In these resonant formulae, it is implicitly assumed that the three S–O bonds are close to a double bond character. The contribution of the structure $\mathbf{III_A}$, which would represent the electron donation of the amide N-atom to the SO_3^- group, should be safely discarded as irrelevant.

Scheme 1

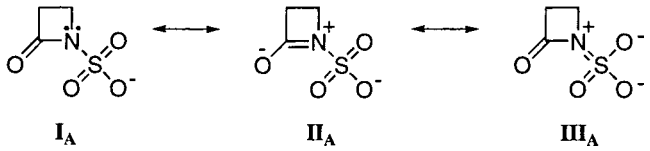

$\mathbf{I_A}$ $\mathbf{II_A}$ $\mathbf{III_A}$

As expected from the presence of the fused thiazolidine ring, the optimized structure of the bicyclic model 3α-carboxypenam shows a significant N pyramidalization (Σ_{angles} X–N–Y = 344.7°, 338.2° in the crystal structure of benzylpenicillin in [30]). With respect to 3-(formylamino)-4-methylazetidin-2-one, the pyramidalized N-atom in 3α-carboxypenam increases its negative charge by 0.23 e and results in moderate changes of the C–N and C=O amide bond lengths of + 0.013 and +0.005 Å, respectively (see *Fig. 1*). In contrast to the monobactam model, these structural and electronic changes reveal a significant destabilization of the amide functionality.

It has been recently proposed that the C=O bond length in β-lactams is a reactivity index that represents the cumulative effect of various factors such as ring strain, ring fusion, substituent on the N-atom, and side chains on the stability of β-lactams [31]. We feel that neither the C=O bond lengths nor the slight changes of the amide group for the structures in *Fig. 1* can satisfactorily explain the differences and similarities in the reactivity of these families of β-lactams. Alternatively, the nature of the negatively charged group and its relative position with respect to the amide functionality could be the major factor influencing the chemical reactivity of these β-lactam models. For example, the monobactam sulfonate group shows a *harder* charge distribution and a closer contact with the reactive amide moiety than the carboxylate group in the penicillin model (see *Fig. 1*). These considerations would be mostly relevant for the stability of the transition structures and intermediates for the breaking or forming of C–N bonds and/or H-shift processes.

3.3. *Reaction Mechanisms.* The exploration of the PES for the reaction between the monobactam model and ammonia rendered four possible pathways for this process, starting with the same prereactive complex. Two of these mechanistic routes, the concerted and the first stepwise mechanism, are quite similar to those previously described for the uncatalyzed ammonolysis of the simplest β-lactam model azetidin-2-

one [9]. In addition, the presence of the *N*-sulfonate group results in two new mechanisms involving the direct participation of this group (see below).

The calculated *Gibbs*-energy profiles and the structures located along the concerted and the three stepwise-reaction paths are shown in *Figs. 2–6*, while the relative energies and the corresponding relative *Gibbs*-energy values, both in the gas phase and in solution, are collected in the *Table*.

Prereactive Complex. The concerted and stepwise reaction paths for the ammonolysis of the monobactam start from the same prereactive complex, which is characterized by a $N-SO_3^- \cdots H-NH_2$ H-bond contact of 2.13 Å with a moderate binding energy of 4.4 kcal/mol (see structure **C** in *Fig. 2*). The lone pair of the ammonia molecule is partially oriented towards the Me-group at C(4), while the internal geometry of the monobactam is practically unaltered, its β-lactam ring being practically planar (Σ_{angles} X–N–Y = 359.9°). The SO_3^- group in **C** binds the ammonia molecule with an orientation favorable to attack the C=O group.

Concerted Mechanism. The nucleophilic attack of NH_3 to the β-lactam C=O group with simultaneous cleavage of the monobactam ring and H transfer to the leaving amino group proceeds through $\mathbf{TS_C}$, which presents a tight structure with reactive C–N bond lengths of *ca.* 1.6–1.7 Å (see *Fig. 2*). The $\Delta G_{gas\text{-}phase}$ of $\mathbf{TS_C}$ is 54.2 kcal/mol, while the corresponding ΔG_{rxn} value of −10.0 kcal/mol indicates moderate thermodynamic driving force for the ammonolysis reaction. Comparing $\mathbf{TS_C}$ with its counterpart in the ammonolysis of azetidin-2-one [9], the presence of the $N-SO_3^-$ moiety results in a moderate decrease of the $\Delta G_{gas\text{-}phase}$ energy barrier of 2.3 kcal/mol. The thermodynamic effect of substituents in the β-lactam ring is only 0.2 kcal/mol in terms of $\Delta G_{gas\text{-}phase}$ values (see *Table*).

Stepwise Mechanism 1. The complex **C** may also evolve through a transition state (TS) for the 1,2-addition of an ammonia N–H bond across the C=O bond ($\mathbf{TS_1}$ in *Fig. 3*). At $\mathbf{TS_1}$, the $[-N-SO_3]^-$ moiety establishes a short $O \cdots H-N$ H-bond [32] with the attacking ammonia (1.82 Å). This secondary role of the SO_3^- group is reflected in the computed $\Delta G_{gas\text{-}phase}$ energy (53.7 kcal/mol), which is 4.4 kcal/mol lower than that observed for the ammonolysis of azetidin-2-one.

$\mathbf{TS_1}$ is connected with a tetrahedral intermediate $\mathbf{I_1}$, which is less stable than separate reactants by 15.3 kcal/mol in terms of $\Delta G_{gas\text{-}phase}$. In this intermediate, the endocyclic N-atom becomes clearly pyramidalized and the OH and SO_3^- groups are linked by a short $O-H \cdots O$ H-bond of 1.72 Å (see *Fig. 2*). The most stable unsubstituted intermediate has a $\Delta G_{gas\text{-}phase}$ value of 10.1 kcal/mol above that of $\mathbf{I_1}$ and shows a more distorted β-lactam ring with an endocyclic C–N distance of 1.55 Å [9]. Thus, the *N*-SO_3^- substitution thermodynamically favors the formation of the tetrahedral intermediate. It may be interesting to note that, in order to stabilize the tetrahedral intermediate by means of this $O-H \cdots O$ interaction, the flexibility of the *N*-SO_3^- group permits the nitrogen inversion along the $\mathbf{TS_1}$ product channel leading to the $\mathbf{I_1}$ structure. Correspondingly, we found that an isomer of $\mathbf{I_1}$,with the OH and SO_3^- groups in *anti* relationship, is not a stable structure on the PES.

The ring opening of $\mathbf{I_1}$ to give the final product can take place through a TS ($\mathbf{TS_2}$ in *Fig. 3*) in which the H-atom is shifted from the O-atom to the N-atom of the β-lactam ring with simultaneous rupture of the endocyclic C–N bond. The $\Delta G_{gas\text{-}phase}$ energy barrier of $\mathbf{TS_2}$ (45.3 kcal/mol) indicates that $\mathbf{TS_1}$ is the kinetically controlling TS for this

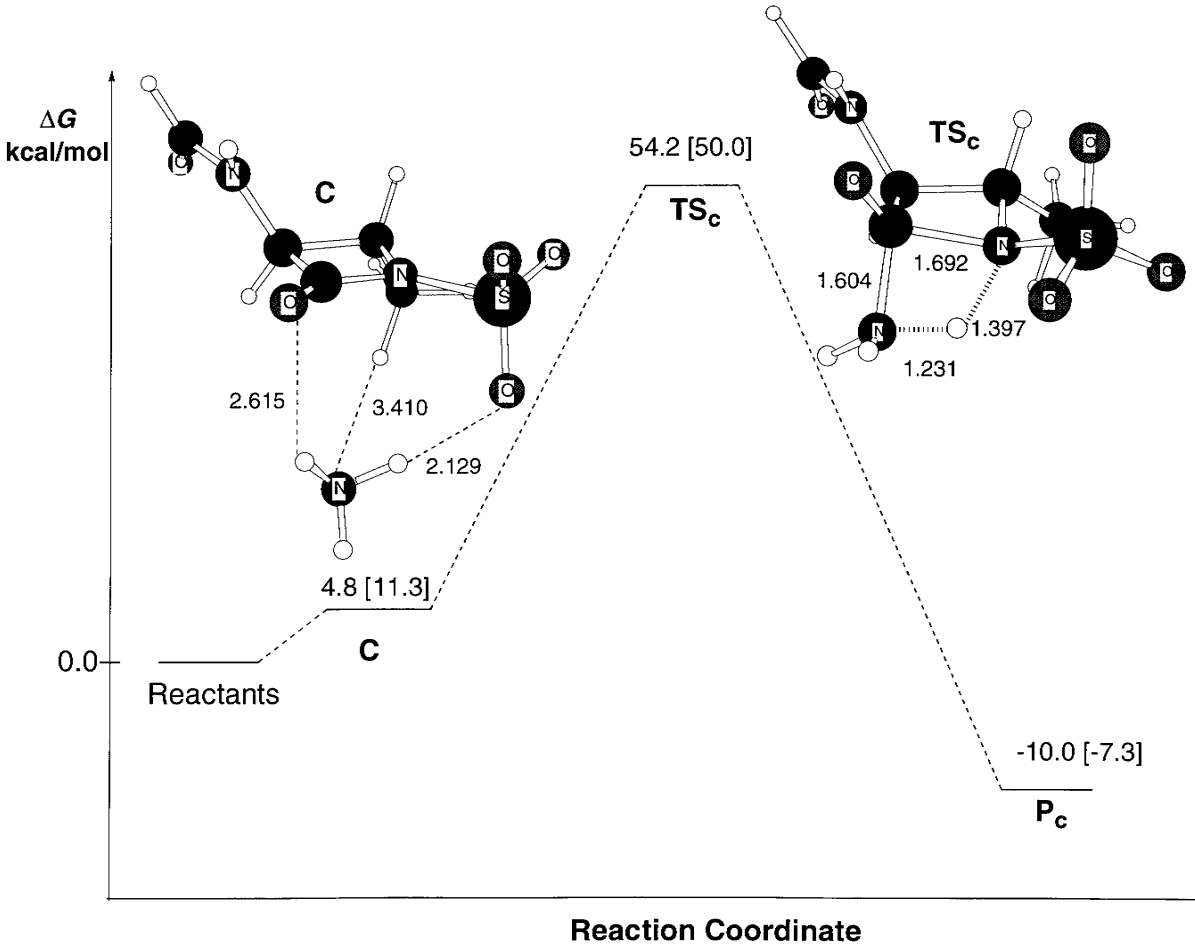

Fig. 2. Gibbs-*energy profiles* [kcal/mol] *both in the gas phase and in solution* (in brackets) *for the concerted reaction channel corresponding to the ammonolysis reaction of 3-(formylamino)-4-methyl-2-oxoazetidine-1-sulfonate*

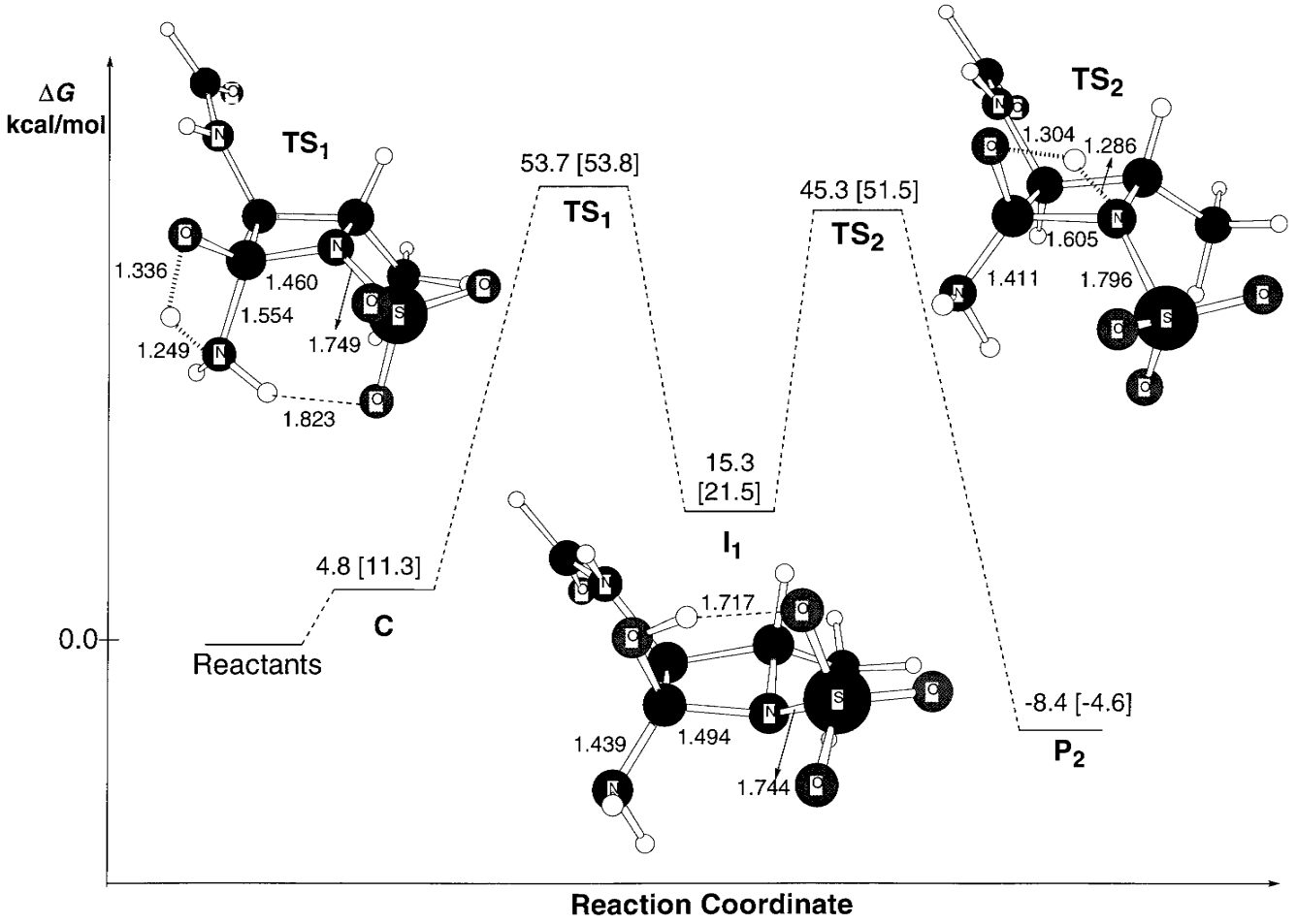

Fig. 3. Gibbs-*energy profiles* [kcal/mol] *both in the gas phase and in solution* (in brackets) *for the first stepwise mechanism*

nonconcerted mechanism. With respect to the analogous TS involved in the ammonolysis of azetidin-2-one [9], the presence of the *N*-SO_3^- group determines a much more reactant-like character of $\mathbf{TS_2}$, with a breaking C–N bond 0.3 Å shorter and a $\Delta G_{\text{gas-phase}}$ energy lower by 7.9 kcal/mol.

For this stepwise mechanism, the resultant product conformer $\mathbf{P_2}$ is by *ca.* 1.6 kcal/mol less stable than $\mathbf{P_C}$. We see again that the *N*-SO_3^- and formylamino groups have a negligible thermodynamic effect, since the calculated reaction *Gibbs* energy coincides with that for the unsubstituted azetidin-2-one (– 8.4 kcal/mol).

Stepwise Mechanism 2. The formation of the tetrahedral intermediate $\mathbf{I_1}$ *via* the $\mathbf{C} \rightarrow \mathbf{TS_1} \rightarrow \mathbf{I_1}$ sequence constitutes the first step of the second stepwise route as well. At $\mathbf{I_1}$, the intramolecular OH···O contact seems particularly appropriate for the transfer of the H-atom from the OH group to the SO_3^- group. This H-transfer and the monobactam ring cleavage can take place through $\mathbf{TS_3}$ in *Fig. 4*, requiring a $\Delta G_{\text{gas-phase}}$ barrier, with respect to $\mathbf{I_1}$, of only 9.6 kcal/mol, 20.4 kcal/mol lower than that of $\mathbf{TS_2}$. The H-atom is practically transferred at $\mathbf{TS_3}$, and the elongation of the endocyclic C–N bond, which has a distance of 1.817 Å, dominates the corresponding transition vector. The $\mathbf{TS_3}$ connects with an open-chain intermediate $\mathbf{I_2}$, which is by 4.6 kcal/mol more stable than its precursor $\mathbf{I_1}$, but by 10.7 kcal/mol less stable than the initial reactants in terms of $\Delta G_{\text{gas-phase}}$.

Resonance structures in *Scheme 2* allow us to understand how the *N*-SO_3^- group induces the β-lactam fission through the relatively stable $\mathbf{TS_3}$. Formally, as a consequence of the proton abstraction by the *N*-SO_3^- moiety, the carbonyl O-atom would become negatively charged, as shown in resonance structure $\mathbf{I_B}$. However, the cleavage of the β-lactam ring and proton transfer leading to the $[-N-SO_3H]^-$ functionality can also stabilize the negative charge as shown in the resonance structures $\mathbf{II_B}$–$\mathbf{IV_B}$. The predominance of $\mathbf{II_B}$–$\mathbf{IV_B}$ is well-reflected in the calculated geometry and charge distribution of $\mathbf{TS_3}$ and $\mathbf{I_2}$, which have a shorter N–S bond (*ca.* 1.6 Å) and a larger negative NPA charge at the N-atom (*ca.* –1.0 e) than those of the tetrahedral intermediate $\mathbf{I_1}$ (1.745 Å, –0.79 e). Note that, effectively, abstraction of a proton does not lead to a *neutral/acid*, but to another *charged/basic* isomer characterized by the presence of the $[-N-SO_3H]^-$ anionic group in consonance with the strong-acid character of the *N*-SO_3^- group.

The intermediate $\mathbf{I_2}$ is practically isoenergetic to the separate reactants ($\Delta E =$ 0.2 kcal/mol; see *Table*). On one hand, the cleavage of the four-membered ring releases the β-lactam strain energy, which amounts to *ca.* 28 kcal/mol for monocyclic β-lactams [9][33]. On the other hand, we expect that the $[-N-SO_3H]^-$ anionic group would be by *ca.* 20 kcal/mol less stable than $-NH-SO_3^-$, as suggested by our test calculations on the $NH_2-SO_3^-$ species. Thus, these opposite energetic factors explain well the null exoergicity for the formation of $\mathbf{I_2}$.

A $[-N-SO_3H]^- \rightarrow -NH-SO_3^-$ isomerization process is required to form the ammonolysis product from $\mathbf{I_2}$ and to release the corresponding reaction energy. The critical structures $\mathbf{TS_i}$, $\mathbf{I_3}$, and $\mathbf{TS_4}$ describe the conversion of $\mathbf{I_2}$ to the final product (see *Fig. 4*). The $\mathbf{TS_i}$ corresponds to a low-barrier conformational TS in which the NH···N interaction between the amido group and the *N*-SO_3H moiety is no more present and a NH···O interaction appears to reach the conformer $\mathbf{I_3}$, in which the OH group is directly oriented towards the N-atom. The $\Delta G_{\text{gas-phase}}$ barrier for the $\mathbf{I_2} \rightarrow \mathbf{I_3}$ trans-

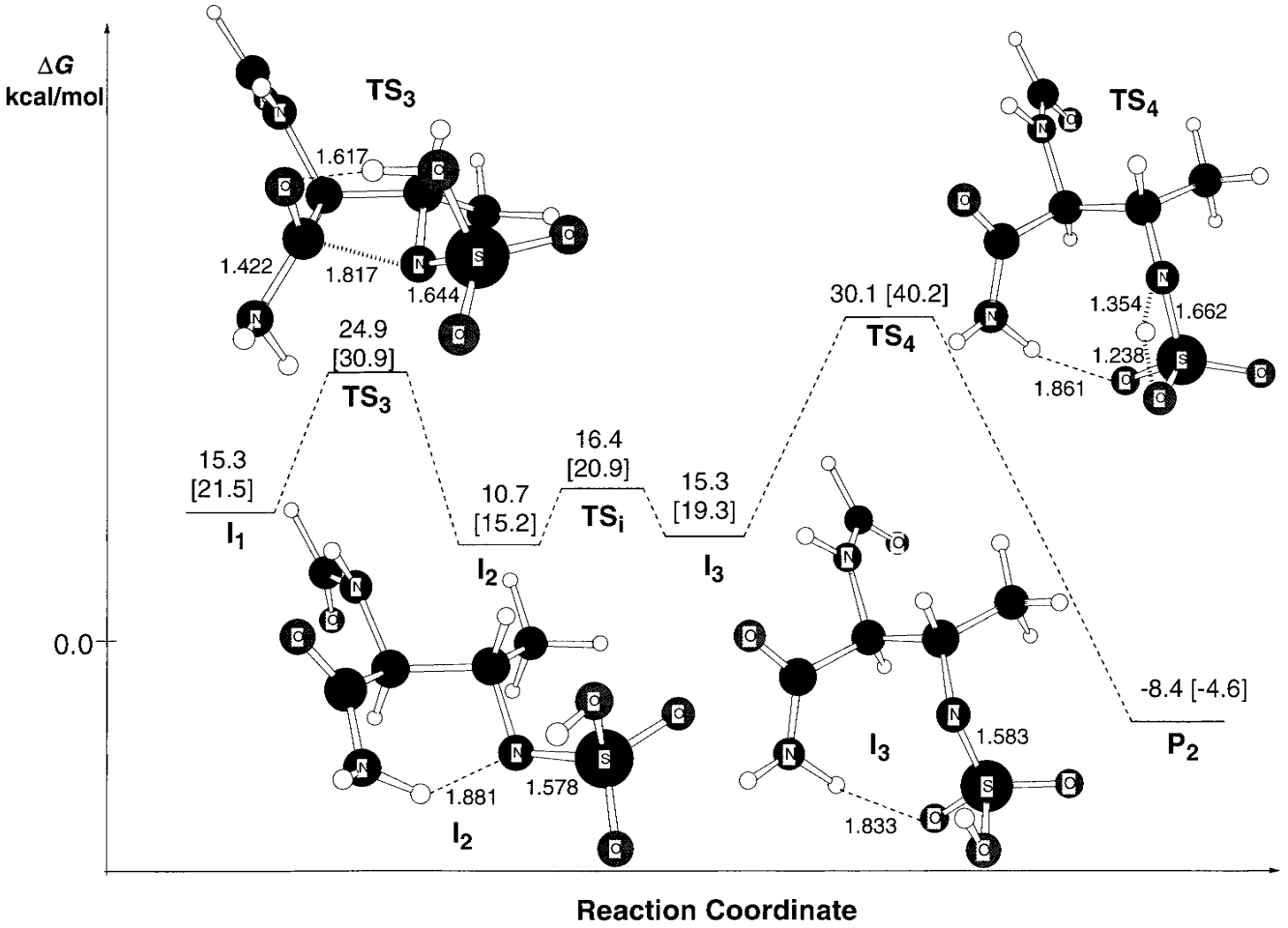

Fig. 4. Gibbs-*energy profiles* [kcal/mol] *both in the gas phase and in solution* (in brackets) *for the second stepwise mechanism*

Scheme 2

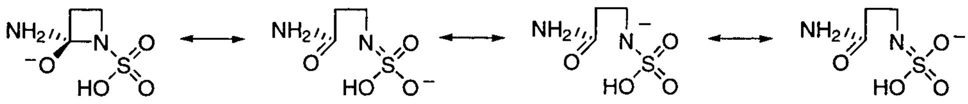

$\mathbf{I_B}$ $\mathbf{II_B}$ $\mathbf{III_B}$ $\mathbf{IV_B}$

formation amounts to 5.7 kcal/mol, the $\mathbf{I_3}$ conformer being less stable by 4.6 kcal/mol. The instability of the $[-N-SO_3H]^-$ moiety results in a moderate energy barrier on going from $\mathbf{I_3}$ to the transition state $\mathbf{TS_4}$. This TS for 1,3 H-shift, which is by 14.8 and 30.1 kcal/mol less stable than $\mathbf{I_3}$ and separate reactants, respectively, is connected on the PES with the product conformer $\mathbf{P_2}$ discussed previously.

Although the direct participation of the N-SO_3^- group as a proton shuttle greatly facilitates the cleavage of the intermediate $\mathbf{I_1}$, we observe that $\mathbf{TS_1}$ is the kinetically controlling TS for this second stepwise mechanism with a rate-limiting activation energy of 53.7 kcal/mol. This value is 24–38 kcal/mol greater than the $\Delta G_{\text{gas-phase}}$ energies of the structures along the $\mathbf{I_1} \rightarrow \mathbf{I_2} \rightarrow \mathbf{I_3} \rightarrow \mathbf{P_2}$ conversion mediated by the N-SO_3^- moiety.

Stepwise Mechanism 3. The closeness of the N-SO_3^- group to the reactive amide bond and the advanced character of the TSs for the ammonolysis of β-lactams with forming C–N bond distances of 1.55–1.66 Å determine the presence of the NH$\cdots$O interaction at $\mathbf{TS_1}$, in which the SO_3^- group plays only a passive role. However, a more active role of the N-SO_3^- group to accept a H-atom from the attacking ammonia molecule should be also feasible. This is confirmed by the location and characterization of $\mathbf{TS_5}$ in *Fig. 5*, which is the first TS of another nonconcerted route specific for the ammonolysis of monobactams.

The $\mathbf{TS_5}$ has geometric characteristics that are intermediate between those of the $\mathbf{TS_1}$ and $\mathbf{TS_3}$ structures, while its transition vector becomes dominated by the H-transfer from the attacking NH_3 to the N-SO_3^- group. At $\mathbf{TS_5}$, the forming C–N bond is much advanced (1.57 Å), the H-atom being transferred lies in the middle position between the donor N- and the acceptor O-atoms, while the endocylic C–N bond is destabilized (1.58 Å). The calculated $\Delta G_{\text{gas-phase}}$ of $\mathbf{TS_5}$ amounts to 37.2 kcal/mol.

From $\mathbf{TS_5}$, the completion of the H-transfer leads to a tetrahedral intermediate $\mathbf{I_4}$ on the B3LYP/6-31 + G* PES, which is by only 0.2 kcal/mol ($\Delta G_{\text{gas-phase}}$) more stable than $\mathbf{TS_5}$. In this intermediate, the presence of the $[-N-SO_3H]^-$ group results in a very distorted β-lactam ring with a C–N distance of 1.685 Å. In consonance with the importance of resonance structures $\mathbf{II_B}$ – $\mathbf{IV_B}$ discussed above, the existence of $\mathbf{I_4}$ can be only transient, since this intermediate is extremely close both in energy and structure to a TS, $\mathbf{TS_6}$, for the total rupture of the endocylic C–N bond. This TS presents a breaking C–N bond length of 1.823 Å and a $\Delta G_{\text{gas-phase}}$ energy barrier of only 0.6 kcal/mol with respect to $\mathbf{I_4}$. The product channel of $\mathbf{TS_6}$ leads to an open-chain intermediate $\mathbf{I_5}$, which is 20.5 kcal/mol below $\mathbf{TS_6}$.

The *Gibbs*-energy profile in *Fig. 5* indicates that the rate-determining activation energy for the formation of $\mathbf{I_5}$ corresponds to that of $\mathbf{TS_6}$, *i.e.* 37.6 kcal/mol. We also see clearly that the $\mathbf{TS_5}$, $\mathbf{I_4}$, and $\mathbf{TS_6}$ structures are very close in energy on the B3LYP/6-31 +

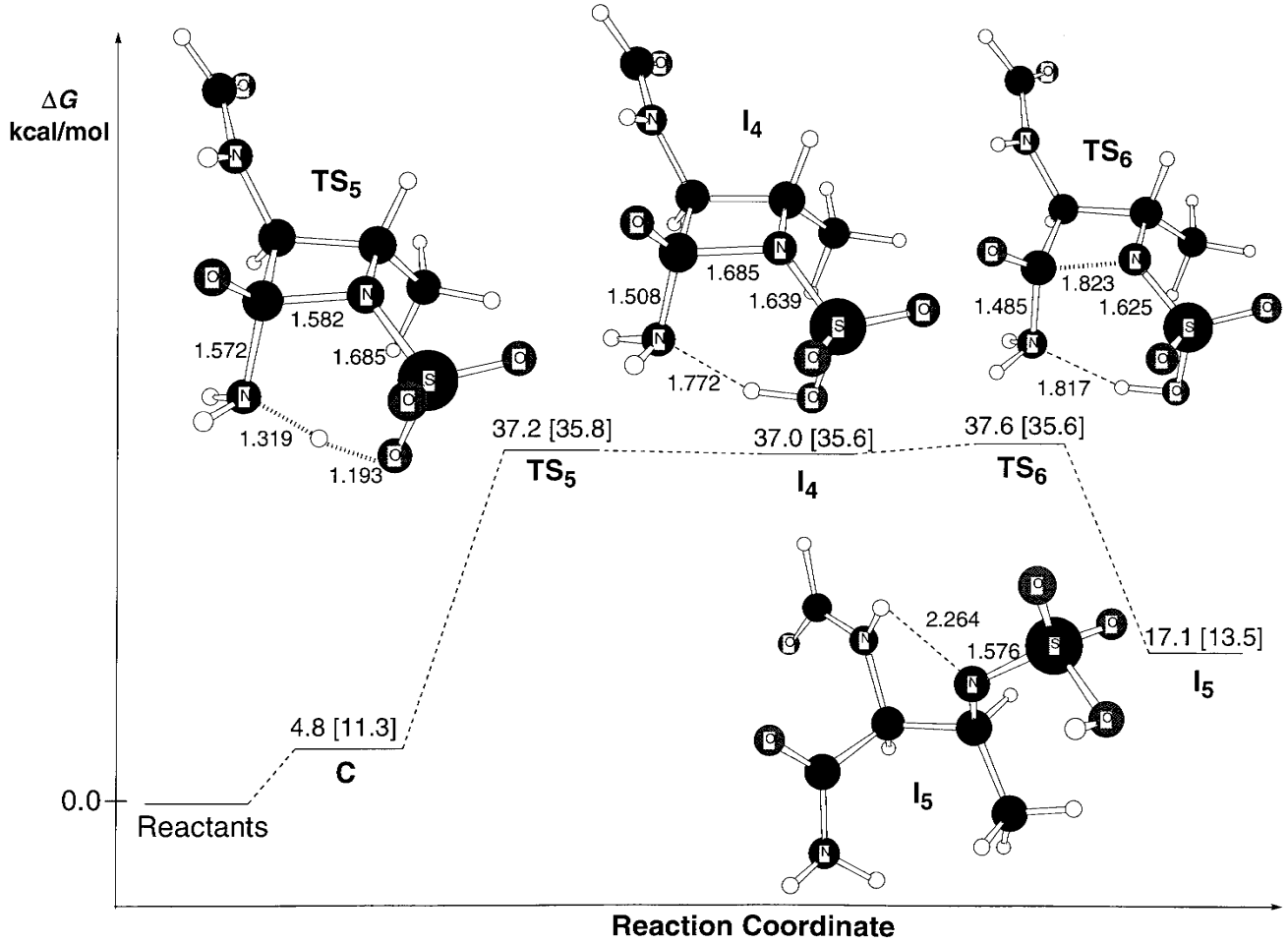

Fig. 5. Gibbs-*energy profiles* [kcal/mol] *both in the gas phase and in solution* (in brackets) *for the formation of the open-chain intermediate along the* N-SO_3^-*-assisted stepwise mechanism*

G* PES. Thus, coalescence of $\mathbf{I_4}$ with either $\mathbf{TS_5}$ or $\mathbf{TS_6}$ could be reasonably expected at other levels of theory. Nevertheless, the series of structures $\mathbf{C} \rightarrow [\mathbf{TS_5}]^{\neq} \rightarrow \mathbf{I_4} \rightarrow [\mathbf{TS_6}]^{\neq} \rightarrow \mathbf{I_5}$ give interesting mechanistic details of the ring opening of the monobactam through the *N*-SO_3^--assisted ammonolysis. This process may be regarded as occurring in three consecutive stages as follows: first the C–N bond is formed by the nucleophilic attack of ammonia at the β-lactam C=O group; second, a H-atom is completely transferred from the ammonia moiety to the SO_3^- group. This second stage destabilizes the monobactam ring as a consequence of the *N*-SO_3^- catalytic effect (see below). Finally, the C–N bond completely breaks by a stretching motion that channels the major part of the monobactam strain energy into the $[-N-SO_3H]^-$ functionality.

$\mathbf{I_5}$ is a conformational isomer of the intermediates $\mathbf{I_2}$ and $\mathbf{I_3}$, in which the formylamino side chain and the SO_3H group present a *syn* relationship (*anti* in $\mathbf{I_2}$ and $\mathbf{I_3}$) stabilized by an intramolecular H-bond connecting these substituents. This intermediate $\mathbf{I_5}$ is by 6.4 and 1.8 kcal/mol less stable than $\mathbf{I_2}$ and $\mathbf{I_3}$, respectively. Several pathways, not detailed here, would be feasible for the evolution of $\mathbf{I_5}$. On the one hand, the *syn* conformation at $\mathbf{I_5}$ could be transformed into the *anti* one at $\mathbf{I_2}$ or $\mathbf{I_3}$ through different low-barrier steps for internal rotations and/or inversion at the N-atom. From the $\mathbf{I_3}$ intermediate, the conversion of the $[-N-SO_3H]^-$ group to the thermodynamically stable $-NH-SO_3^-$ form *via* $\mathbf{TS_4}$, would render the product complex $\mathbf{P_2}$. Alternatively, the formation of the final product can also take place maintaining the *syn* orientation of the formylamino and the *N*-SO_3^- group. *Fig. 6* displays a reaction pathway for this process in which a *syn* intermediate $\mathbf{I_6}$, which is accessible from $\mathbf{I_5}$ by sequences of low-barrier internal rotations, is directly connected with $\mathbf{TS_7}$ for the $[-N-SO_3H]^- \rightarrow -NH-SO_3^-$ conversion. $\mathbf{TS_7}$, which is 1.8 kcal/mol above its conformational isomer $\mathbf{TS_4}$, has a $\Delta G_{\text{gas-phase}}$ barrier of 31.9 kcal/mol. The resultant product complex $\mathbf{P_3}$ is by 10.4 kcal/mol more stable than reactants.

For this third stepwise mechanism, we note that the rate-determining energy barrier corresponds to that of $\mathbf{TS_6}$ (37.6 kcal/mol) involved in the cleavage of the β-lactam ring. The different TSs for the $[-N-SO_3H]^- \rightarrow -NH-SO_3^-$ conversion, $\mathbf{TS_4}$ and $\mathbf{TS_7}$, have energy barriers by 7.5 kcal/mol and 5.7 kcal/mol lower than that of $\mathbf{TS_6}$, respectively. Thus, the sequence of chemical events along this stepwise mechanism renders an efficient route for the cleavage of the monobactam, the rate-determining energy barrier being by *ca.* 16 kcal/mol lower than those for other mechanisms.

3.4. *Continuum Solvent Effects.* In aqueous solution, the transition state $\mathbf{TS_C}$ becomes stabilized with a $\Delta\Delta G_{\text{solvation}}$ value of -4.2 kcal/mol, as expected from its bare accumulation of negative charge in the carbonyl O-atom and in the SO_3^- group. Thus, $\mathbf{TS_C}$ is by 3.8 kcal/mol more stable than $\mathbf{TS_1}$, which is the rate-determining TS of the first and second stepwise mechanisms. Cleavage of the monobactam model catalyzed by the *N*-SO_3^- group is also predicted to be slightly favored by 1–4 kcal/mol due to solvent effects (see *Table*). In addition, the solvent continuum reverses the *syn*/*anti* preference of the open-chain intermediates and destabilizes moderately the final step for the formation of the $-NH-SO_3^-$ group, leading to the product complexes $\mathbf{P_2}$ and $\mathbf{P_3}$. The calculated energy barriers for $\mathbf{TS_4}$ and $\mathbf{TS_7}$ in solution amount to 40.2 and 39.7 kcal/mol, respectively, these figures being around 4 kcal/mol above the $\Delta G_{\text{solution}}$ values for the $\mathbf{C} \rightarrow [\mathbf{TS_5}]^{\neq} \rightarrow \mathbf{I_4} \rightarrow [\mathbf{TS_6}]^{\neq} \rightarrow \mathbf{I_5}$ conversion. The kinetic preference for the *N*-SO_3^--assisted mechanism observed in the gas-phase energy profiles is not

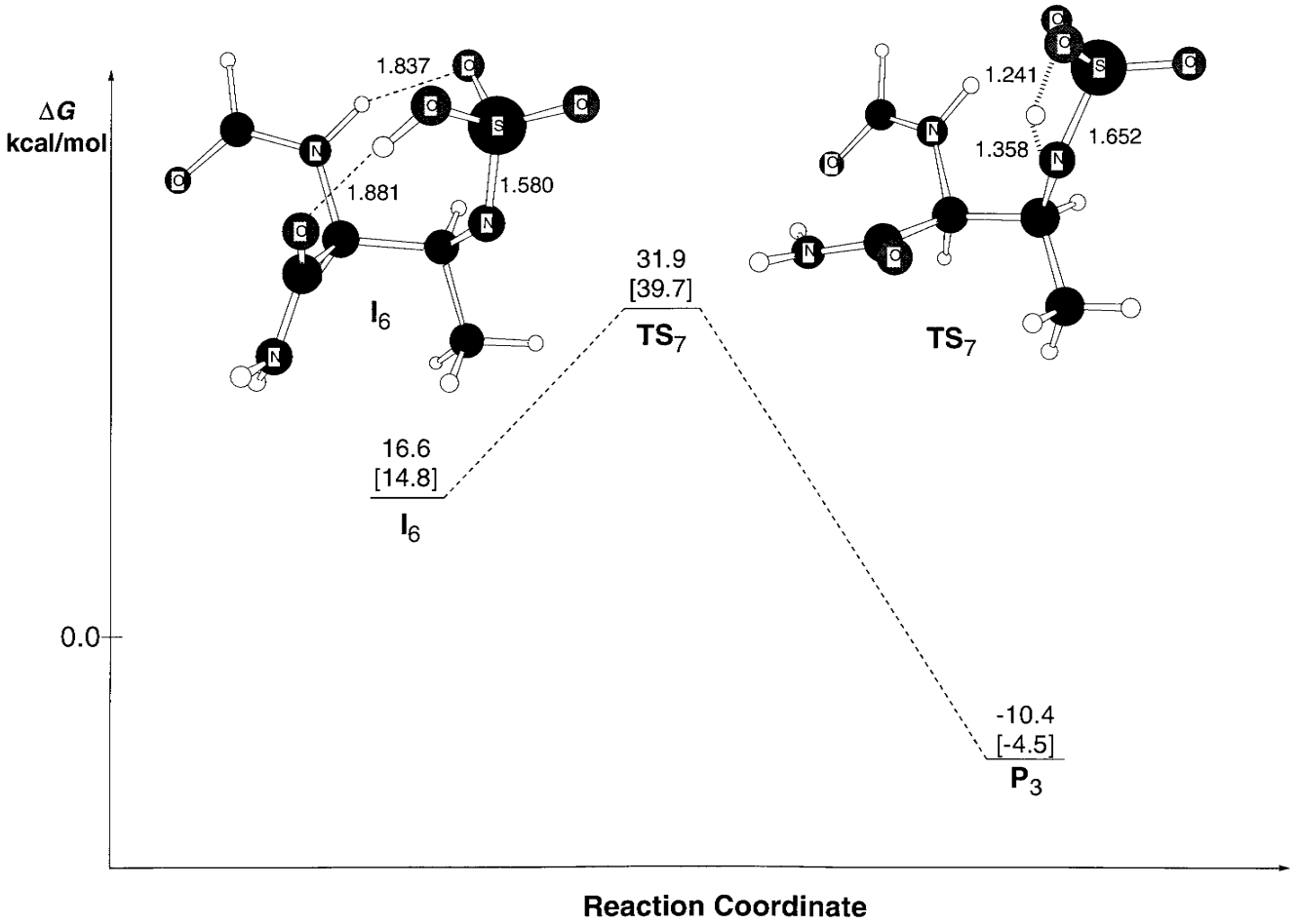

Fig. 6. Gibbs-*energy profiles* [kcal/mol] *both in the gas phase and in solution* (in brackets) *for the evolution of the* syn *open-chain intermediate along the* N-SO_3^-*-assisted stepwise mechanism*

modified in solution, since the rate-determining $\Delta G_{solution}$ barrier for the third stepwise mechanism remains much lower than those of $\mathbf{TS_C}$ and $\mathbf{TS_1}$.

3.5. *Intramolecular Catalysis by the* N-*Sulfonate Group*. Owing to its poor basicity, the *N*-SO_3^- group does not act as a base catalyst. In fact, the origin of the intramolecular catalysis due to the *N*-SO_3^- group is closely related to the electronic rearrangement involved in the $-NH-SO_3^- \rightarrow [-N-SO_3H]^-$ isomerization. This process, which connects two basic forms, favors the rupture of the β-lactam ring at the tetrahedral intermediate configurations (see *Scheme 2*). This mechanism of action is quite different from that theoretically observed [10], when a H_2O molecule exerts acid/base bifunctional catalysis [34] on the aminolysis of azetidin-2-one. In terms of $\Delta G_{gas\text{-}phase}$ energies, the catalytic effect of the water molecule is around 12 kcal/mol [10], lower than the 20 kcal/mol due to *N*-sulfonate in the ammonolysis of the monobactam.

3.6. *Comparison with the Aminolysis Reaction of Penicillins.* We have previously studied at the B3LYP/6-31 + G* level of theory the H_2O-assisted aminolysis of 3α-carboxypenam, a penicillin model compound, by concerted and stepwise mechanisms [10]. In the stepwise process, which is the most favored one in the gas phase with a ΔG barrier of 31.0 kcal/mol, both the β-lactam carboxylate group and an ancillary H_2O molecule are required to relay the proton from the attacking nucleophile to the forming amino group. In contrast, the assistance by the *N*-SO_3^- group does not necessarily imply the participation of additional H_2O molecules thanks to its closeness to the reactive amide bond. In the condensed phase, the concerted H_2O-assisted route for the aminolysis of 3α-carboxypenam becomes more favorable due to the strong influence of the environment polarity (*e.g.*, $\Delta\Delta G_{solvation}$ values differed by up to 30 kcal/mol among the different critical structures) [10]. This contrasts sharply with the moderate effects of solvation in the reaction profiles for the ammonolysis of the monobactam model (*ca.* 2 kcal/mol). The computed $\Delta G_{solution}$ barrier for the aminolysis of 3α-carboxypenam is 54.0 kcal/mol with respect to separate reactants (*i.e.*, carboxypenam + CH_3NH_2 + H_2O), 49.7 kcal/mol with respect to carboxypenam + $[CH_3NH_2 \cdots H_2O]$. These values are 10–14 kcal/mol above the $\Delta G_{solution}$ barrier for the ammonolysis of the monobactam model[2]). Therefore, we conclude that, in aqueous solution, monobactams will show an intrinsic reactivity against amine nucleophiles more important than that of penicillins.

3.7. *Significance for the Comparative Immunochemistry of Penicillins and Monobactams.* Let us to briefly review some basic aspects of the immunochemistry of β-lactams in order to further discuss the possible significance of our theoretical results. It is normally accepted that drugs with a low molecular weight cannot stimulate an immune response unless they bind covalently to proteins to form protein-drug conjugates [35]. For β-lactam antibiotics, an essential process of their immunochemistry [17][18] consists of the aminolysis reaction with amino groups of plasma proteins, most importantly with those of the HSA, which is the most abundant plasma protein [36]. Benzylpenicillin, which can potentially elicit a strong immunogenic response [35], binds *specifically* to only six lysine residues (of a total of 59) in the HSA protein [37].

---

[2]) We note that inclusion of amine substituent effects can significantly reduce the energy barrier for the aminolysis reaction with respect to that of ammonolysis. For example, the electron-donor ability of the Me group in the attacking amine stabilizes the $\mathbf{TS_1}$ and $\mathbf{TS_c}$ structures for the aminolysis of azetidin-2-one in *ca.* 4–6 kcal/mol by reinforcing the charge transfer from the amine to the azetidin-2-one (see [9]).

Remarkably, the most reactive lysine residue, Lys199, is located strategically in the so-called IIA hydrophobic pocket in HSA, which has affinity for small, negatively charged hydrophobic molecules like benzylpenicillin [36].

It is also known that the most abundant antibodies recognize the originally bicyclic part of penicillins (*nuclear* antibodies) [18]. This explains the large cross-reactivity observed between penicillins and the structurally related cephalosporins, which can be recognized by the same kind of *nuclear* antibodies [17][18]. More specific antibodies, which discriminate among the different side chains of penicillins, contribute also to the immune response. This *side-chain* specificity of β-lactam-induced antibodies is normally associated with a low potential cross-reaction ability [18]. On the other hand, monobactam antibiotics like aztreonam have been reported to be weakly immunogenic. It has also been shown that the antibodies oriented to the recognition of protein-monobactam conjugates have only side-chain-specific character, explaining, thus the lack of cross-reactivity with penicillins [12][18].

Consideration of either the nature of the noncovalent protein-β-lactam complexes or the nature of the aminolysis mechanisms of β-lactams will be required to understand the comparative immunochemistry of monobactams (aztreonam) and penicillins. For example, aztreonam has a polar side chain bearing a positive charge, and, therefore, it is reasonable to expect that its binding to the hydrophobic IIA site in HSA would be much weaker than that of penicillins or cephalosporins, which have a neutral hydrophobic side chain. In addition, our theoretical analyses have revealed substantial differences in the reactions of penicillins and monobactams with amine nucleophiles: owing to their enhanced reactivity against amino groups, monobactams would not discriminate so much among the different protein lysine residues as do penicillins. Therefore, we propose that, with respect to the reaction between HSA and penicillin, a larger variety of HSA-monobactam conjugates preferentially distributed over the hydrophilic protein surface will be formed. In such a scenario, the lower *specificity* in the reaction between HSA ε-amino groups and monobactam molecules is consistent with the weaker immunogenic response against monobactams as observed experimentally. Interestingly, this proposal seems consistent with the experimental rate for aztreonam conjugation to HSA (70% of the initial aztreonam fixed to HSA after 24 h of reaction as cited in [16]), which is significantly higher than that reported for benzylpenicillins [38] (3% conjugation after 48 h).

We are grateful to *MEC* (Spain) for financial support (PB97-1300). *N. D.* also thanks *MEC* for her grant PB98-44430549.

Supporting Information Available. Figure showing the B3LYP/6-31 + G* structures and atomic charges for all the critical structures involved in the ammonolysis reaction of 3-(formylamino)-4-methyl-2-oxoazetidine-1-sulfonate. Cartesian coordinates for all the critical structures (12 pages). See any current masthead page for ordering information and Internet access instructions.

REFERENCES

[1] 'The Chemistry of β-Lactams', Ed. M. I. Page, Blackie Academic & Professional, London, 1992.
[2] B. B. Levine, Z. Ovary, *J. Exp. Medicine* **1961**, *114*, 875.
[3] A. Saxon, G. N. Beall, A. S. Rohr, D. C. Adelman, *Ann. Int. Med.* **1987**, *107*, 204.

[4] M. I. Page, 'The Mechanism of Reactions of β-Lactams' in 'The Chemistry of β-Lactams', Ed. M. I. Page, Blackie Academic & Professional, London, 1992, pp. 129–147.
[5] G. M. Blackburn, J. D. Plackett, *J. Chem. Soc., Perkin Trans. 2* **1973**, 981.
[6] T. Yamana, A. Tsuji, E. Miyamoto, E. Mira, *J. Pharm. Pharmacol*. **1975**, *27*, 56.
[7] N. P. Gensmantel, M. I. Page, *J. Chem. Soc., Perkin Trans. 2* **1979**, 137.
[8] J. J. Morris, M. I. Page, *J. Chem. Soc., Perkin Trans. 2* **1980**, 220.
[9] N. Díaz, D. Suárez, T. L. Sordo, *Chem. Eur. J.* **1999**, *5*, 1045.
[10] N. Díaz, D. Suárez, T. L. Sordo, *J. Am. Chem. Soc.* **2000**, *122*, 6710.
[11] R. B. Sykes, C. M. Cimarusti, D. P. Bonner, K. Bush, D. M. Floyd, N. H. Georgopapadakou, W. H. Koster, W. C. Liu, W. L. Parker, P. A. Principe, M. L. Rathnum, W. A. Slusarchyk, W. H. Trejo, J. S. Wells, *Nature* **1981**, *291*, 489.
[12] W. C. Hellinger, N. S. Brewer, *Mayo Clin. Proc.* **1999**, *74*, 420.
[13] Z. Wang, W. Fast, A. M. Valentine, S. J. Benkovic, *Curr. Opin. Chem. Biol.* **1999**, *3*, 614.
[14] K. Bush, *Clin. Infect. Diseases* **1998**, *27*, S48.
[15] I. Heinze-Krauss, P. Angehrn, R. L. Charnas, K. Gubernator, E. M. Gutknecht, C. Huschwerlen, M. Kania, C. Oefner, M. C. P. Page, S. Sogabe, J. L. Specklin, F. Winkler, *J. Med. Chem.* **1998**, *41*, 3961.
[16] N. F. Adkinson, E. Swaab, A. A. Sugerman, *Antimicrob. Agents Chemother.* **1984**, *23*, 93.
[17] M. Blanca, J. M. Vega, J. García, A. Miranda, M. J. Carmona, C. Juárez, J. Terrados, J. Fernández, *Clin. Exp. Allergy* **1994**, *24*, 407.
[18] N. F. Adkinson, A. Saxon, M. R. Spence, E. A. Swabb, *Rev. Infect. Diseases* **1985**, *7*, S613.
[19] W. J. Hehre, L. Radom, J. A. Pople, P. v. R. Schleyer, 'Ab Initio Molecular Orbital Theory', John Wiley & Sons Inc. New York, 1986.
[20] A. D. Becke, 'Exchange-Correlation Approximation in Density-Functional Theory', in 'Modern Electronic Structure Theory Part II', Ed. D. R. Yarkony, Ed. World Scientific. 1995, Singapore
[21] Gaussian 98, Revision A.6, M. J. Frisch, G. W. Trucks, H. B. Schlegel, G. E. Scuseria, M. A. Robb, J. R. Cheeseman, V. G. Zakrzewski, J. A. Montgomery Jr., R. E. Stratmann, J. C. Burant, S. Dapprich, J. M. Millam, A. D. Daniels, K. N. Kudin, M. C. Strain, O. Farkas, J. Tomasi, V. Barone, M. Cossi, R. Cammi, B. Mennucci, C. Pomelli, C. Adamo, S. Clifford, J. Ochterski, G. A. Petersson, P. Y. Ayala, Q. Cui, K. Morokuma, D. K. Malick, A. D. Rabuck, K. Raghavachari, J. B. Foresman, J. Cioslowski, J. V. Ortiz, B. B. Stefanov, G. Liu, A. Liashenko, P. Piskorz, I. Komaromi, R. Gomperts, R. L. Martin, D. J. Fox, T. Keith, M. A. Al-Laham, C. Y. Peng, A. Nanayakkara, C. Gonzalez, M. Challacombe, P. M. W. Gill, B. Johnson, W. Chen, M. W. Wong, J. L. Andres, C. Gonzalez, M. Head-Gordon, E. S. Replogle, and J. A. Pople, *Gaussian, Inc.*, Pittsburgh PA, 1998.
[22] K. Fukui, *Acc. Chem. Res.* **1981**, *14*, 363.
[23] D. A. McQuarrie, 'Statistical Mechanics', Harper & Row, New York, 1976.
[24] L. A. Curtiss, P. C. Redfem, B. J. Smith, L. Radom, *J. Chem. Phys.* **1996**, *104*, 5148.
[25] V. Barone, M. Cossi, J. Tomasi, *J. Chem. Phys.* **1997**, *107*, 3210.
[26] J. Tomasi, M. Persico, *Chem. Rev.* **1994**, *94*, 2027.
[27] C. S. Pomelli, J. Tomasi, *J. Phys. Chem. A* **1997**, *101*, 3561.
[28] A. E. Reed, R. B. Weinstock, F. Weinhold, *J. Chem. Phys.* **1985**, *83*, 735.
[29] J. A. Sowek, S. B. Singer, S. Ohringer, M. F. Malley, T. J. Dougherty, J. Z. Gougotas, K. Bush, *Biochemistry* **1991**, *30*, 3179.
[30] I. Csöregh, T. B. Palm, *Acta Crystallogr., Sect. B.* **1977**, *33*, 2169.
[31] I. Massova, P. A. Kollman, *J. Phys. Chem. B.* **1999**, *10*, 8628.
[32] J. A. Gerlt, M. M. Kreevoy, W. W. Cleland, P. A. Frey, *Chem. Biol.* **1997**, *4*, 259.
[33] M. V. Voux, P. Jiménez, J. Z. Dávalos, O. Castaño, M. T. Molina, R. Notario, M. Herreros, J.-L. M. Abboud, *J. Am. Chem. Soc*. **1996**, *118*, 12735.
[34] H. Dugas, 'Bioorganic Chemistry. A Chemical Approach to Enzyme Action', Springer-Verlag, New York, 1996.
[35] B. A. Baldo, N. H. Pham. *Chem. Res. Toxicol*. **1994**, *7*, 703.
[36] T. Peters, 'All about Albumin: Biochemistry, Genetics, and Medical Applications', Academic Press, San Diego, 1996.
[37] a) M. Yvon, P. Anglade, J. M. Val, *FEBS Lett.* **1990**, *263*, 237; b) M. Yvon, P. Anglade, J. M. Val, *FEBS Lett.* **1989**, *247*, 273; c) M. Yvon, P. Anglade, J. M. Val, *FEBS Lett.* **1988**, *239*, 237.
[38] F. R. Batchelor, J. M. Dewdney, D. Gazzard, *Nature* **1965**, *206*, 362.

Received August 24, 2001